Ionics (2019) 25:4607–4614
https://doi.org/10.1007/s11581-019-03012-6

ORIGINAL PAPER

Effect of drying temperature on properties of lithium-rich manganese-based materials in sol-gel method

Changkun Song [1] · Wangjun Feng [1,2] · Zhaojiao Shi [1] · Xuan Wang [1,2]

Received: 7 March 2019 / Accepted: 10 April 2019 / Published online: 21 May 2019

Abstract

A lithium-rich manganese-based cathode material $Li_{1.2}Mn_{0.54}Ni_{0.13}Co_{0.13}O_2$ is restricted by the first charge and discharge efficiency and the cycle retention rate. In this paper, the effects of different drying temperatures on the comprehensive properties of $Li_{1.2}Mn_{0.54}Ni_{0.13}Co_{0.13}O_2$ materials in sol-gel method were studied systematically. Through XRD, SEM, TEM, and electrochemical performance tests, it was found that the prepared materials have the best structure and properties when the drying temperature is 140 °C. The first discharge specific capacity is as high as 262.5 mAh/g in a voltage of 2.0–4.8 V. After circulating 100 cycles at a magnification of 0.5 C and 2 C, the capacity retention ratios were 80.46% and 84.14%, respectively.

Keywords Li-rich · Lithium-ion batteries · Drying temperature · Capacity retention

Introduction

With the advancement of science and technology and the rapid development of human society and the accelerating process of industrialization, people's demand for energy is growing. Conventional secondary batteries are difficult to meet the current demand for higher performance of batteries for electronic products and new energy vehicles [1–5]. At present, the cathode materials for lithium-ion batteries are mainly composed of a layered positive electrode material, including lithium cobaltate ($LiCoO_2$), lithium nickelate ($LiNiO_2$); lithium manganate with spinel structure ($LiMn0_2$); two-ternary composite layered positive electrode material ($LiNi_xCo_yMn_zO_2$); and olivine structure lithium iron phosphate ($LiFePO_4$) and the like [6–10].

In recent years, lithium-rich layered oxide $xLi_2MnO_3\cdot(1-x)LiMO_2 (0 < x < 1$, M = Ni, Co, Mn) has received extensive attention as a promising cathode material because it can generate a capacity (> 250 mAh/g) beyond the redox calculation of transition metal elements in a layered material when charged above 4.5 V [11–13]. However, the study found that the first irreversible capacity loss of this kind of material is large, the first cycle efficiency is low, and its cycle stability and rate performance are not ideal, which limits its application and development. In response to the above problems, many literatures have been reported [14, 15]. These disadvantages for the lithium-rich manganese-based positive electrode material can be modified in the preparation process. The main methods are the feeding method, the pH value control, the reaction temperature, and the sintering temperature.

The ratio of the two components (Li_2MnO_3 and $LiMO_2$) in the lithium-rich manganese-based cathode material plays a key role in the performance of the material, and the different process conditions in the synthesis process are important to the crystal structure and electrochemical performance of the material [2, 16]. Therefore, it is important to explore and study the preparation process and conditions of the materials and the proportion of the components on the physicochemical properties and electrochemical properties of the materials. The lithium-rich manganese-based cathode material $Li_{1.2}Mn_{0.54}Ni_{0.13}Co_{0.13}O_2$ has the advantages of large specific capacity, low preparation cost, and environmental friendliness, and is considered to be the most suitable cathode material for the next generation of lithium-ion batteries [17]. The preparation of lithium-rich manganese-based cathode material by sol-gel method has many advantages such as high purity, low synthesis temperature, short synthesis time,

✉ Wangjun Feng
wjfeng@lut.cn

[1] School of Science, Lanzhou University of Technology, Lanzhou 730050, China

[2] State Key Laboratory of Advanced Processing and Recycling Nonferrous Metals, Lanzhou University of Technology, Lanzhou 730050, China

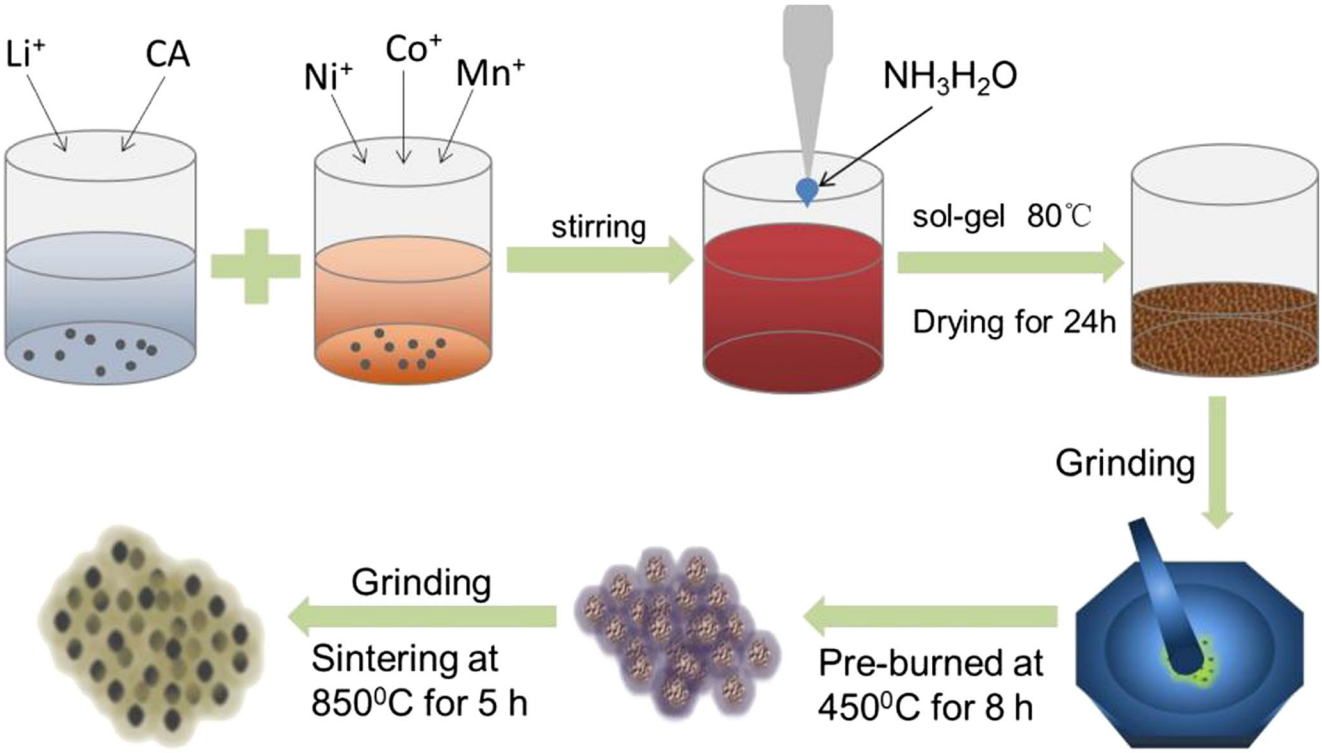

Fig. 1 Schematic diagram of the formation process of materials

small particle size, narrow particle size distribution, good uniformity, and large specific surface area. It is a common method for preparing cathode materials for lithium-ion batteries [18, 19]. Drying temperature is an important factor affecting the sol-gel reaction process. When the drying temperature is low, the synthesized precursor particles are fine and the morphology is irregular; when the drying temperature is too high, the synthesized precursor particles are also small, but the distribution is uneven and the agglomeration is serious. Only precursors synthesized at a suitable temperature have a relatively good morphology and a uniform distribution.

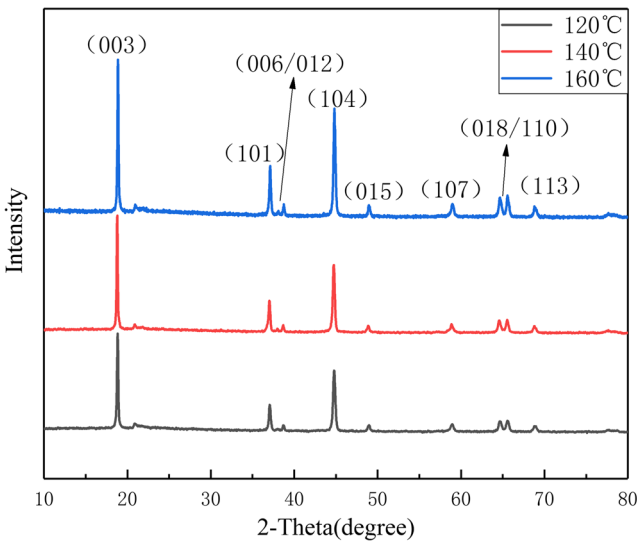

Fig. 2 XRD patterns of various $Li_{1.2}Mn_{0.54}Ni_{0.13}Co_{0.13}O_2$ at different drying temperatures

For a series of problems, we prepared a lithium-rich manganese-based cathode material $Li_{1.2}Mn_{0.54}Ni_{0.13}Co_{0.13}O_2$ by sol-gel method. And systematically study the effect of drying temperature on its performance. First, we prepared materials with drying temperatures of 120 °C, 140 °C, and 160 °C, respectively. Then, the crystal structure, morphology, and electrochemical properties of each material were tested. Finally, the data obtained were characterized and analyzed. We conclude that the resulting material has the best performance when the drying temperature is 140 °C. The first charge–discharge specific capacity reached 338.0 mAh/g and 262.5 mAh/g at 0.1 C, respectively. Furthermore, it showed a high discharge capacity of 200.1 mAh/g and 158.9 mAh/g at 0.5 C and 2 C and capacity retention of 80.46% and 84.14% after 100 cycles, respectively.

Experimental

Material preparation

The lithium-rich layered oxide material $Li_{1.2}Mn_{0.54}Ni_{0.13}Co_{0.13}O_2$ was synthesized using a modified sol-gel method. $Mn(CH_3COO)_2{\cdot}4H_2O$, $Ni(CH_3COO)_2{\cdot}4H_20$, $Co(CH_3COO)_2{\cdot}$

Table 1 Lattice parameters of the different drying time samples

Samples	*a* (Å)	*c* (Å)	*c*/*a*	$I_{(003)}/I_{(104)}$
120 °C	2.8457	14.1310	4.9657	1.53
140 °C	2.8460	14.1750	4.9806	1.64
160 °C	2.8451	14.1059	4.9579	1.42

$4H_2O$ were dissolved in a certain amount of deionized water at a stoichiometric ratio of 54:13:13 to be referred to as solution A. Then, $CH_3COOLi{\cdot}2H_2O$ and $C_6H_8O_7{\cdot}H_2O$ were dissolved in deionized water at a molar ratio of 6:5 to form solution B. Next, solution A was slowly added dropwise to the solution B and continuously stirred, and then the aqueous ammonia was added dropwise to adjust the pH to 9 to obtain a mixed solution. The obtained mixed solution was placed in a water bath at 80 °C and stirred to obtain a gelatinous substance, which was then placed in a dry box and dried at 120 °C, 140 °C, and 160 °C for 24 h to obtain three products. Finally, the dried material was ground and placed in a tube furnace and calcined at 450 °C for 8 h, and then the grinding was continued, followed by re-baking in a tube furnace at a high temperature of 850 °C for 5 h to obtain the final sample (Fig. 1).

Material characterization

X-ray diffraction (XRD) measurements of materials were using Bruker D8 Advance diffractometer with Cu Kα radiation. The range of diffraction data collection is $10° < 2\theta < 80°$. The morphological characteristics of the samples were observed by scanning electron microscope (SEM) JSM-6700F, whose acceleration voltage was 20 KV. The TEM images of the samples were JEM-2100F collected at 200 KV. High-resolution transmission electron microscopy (HRTEM) was performed on a Philips Tecnai 20U-TWIN microscope at 300 KV.

Preparation of cathode and electrochemical analysis

The electrochemical characterization was performed using CR2032 coin cells with lithium metal as the counter electrode. The positive electrode was prepared by mixing the as-synthesized cathode material $Li_{1.2}Mn_{0.54}Ni_{0.13}Co_{0.13}O_2$, acetylene black (conductive agent) and polyvinylidene fluoride (PVDF), were dissolved in 1-methyl-2-pyrrolidone (NMP) with a weight ratio of 8:1:1. The slurry was uniformly applied to an aluminum foil and then dried under vacuum at 55 °C for 12 h. The obtained positive electrode was cut into a disk having a diameter of 14 mm. The half-cell consists of positive electrode material and lithium metal negative electrode separated by a Celgard 2400 polyethylene/polypropylene film, assembled in a sealed argon-filled glove box. The electrolyte was prepared by dissolving 1 M LiPF6 in EC/DMC/DEC (1:1:1 volume). The charge–discharge test was carried out using the Land-CT2001A Battery Test System (Wuhan, China) with a voltage range of 2.0 V–4.8 V. Electrochemical impedance spectroscopy (EIS) and cyclic voltammetry (CV) studies were performed at electrochemical workstations. The electrochemical

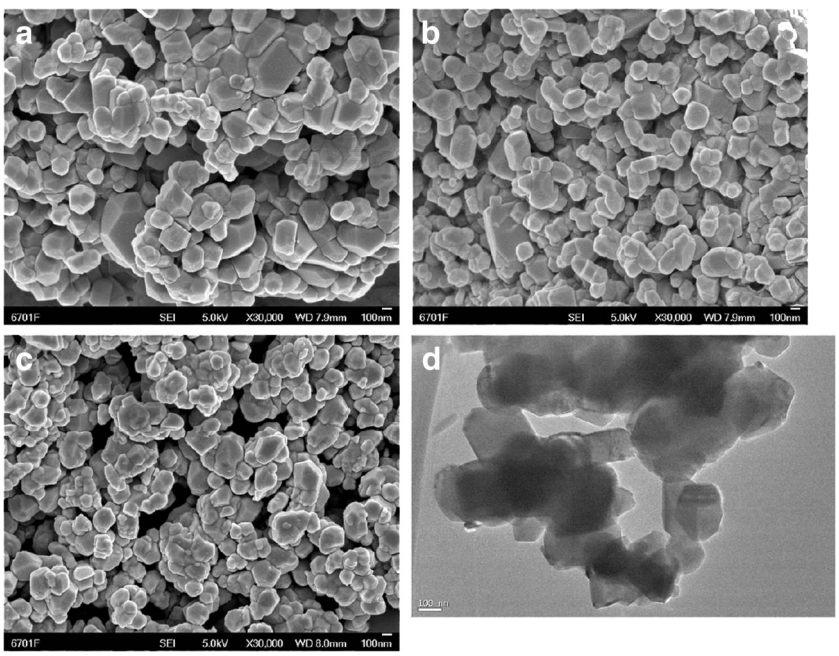

Fig. 3 SEM images of $Li_{1.2}Mn_{0.54}N\ i_{0.13}Co_{0.13}O_2$ at **a**120 °C, **b** 140 °C, and **c** 160 °C. TEM images of $Li_{1.2}Mn_{0.54}Ni_{0.13}Co_{0.13}O_2$ at **d** 140 °C

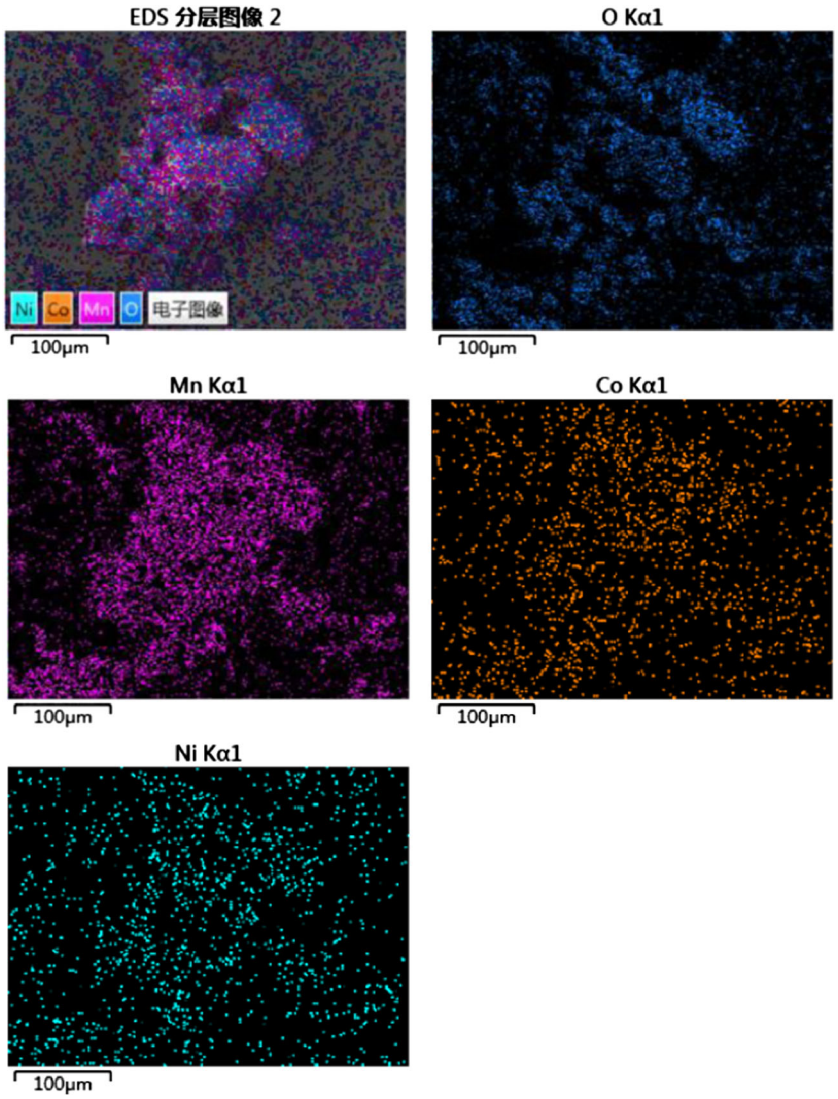

Fig. 4 EDS mapping of Ni, Co, and Mn based on the $Li_{1.2}Mn_{0.54}Ni_{0.13}Co_{0.13}O_2$ material at drying temperature of 140 °C

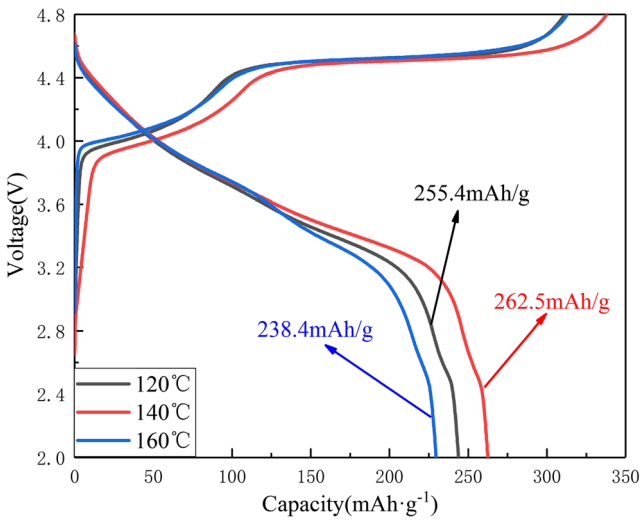

Fig. 5 The first charge and discharge curve of the sample

impedance spectroscopy (EIS) has a test frequency of 100 kHz to 10 mHz and a perturbation amplitude of 5 mV.

Results and discussion

Crystalline structure analysis

Figure 2 is the XRD pattern of the $Li_{1.2}Mn_{0.54}Ni_{0.13}Co_{0.13}O_2$ material at drying temperatures of 120 °C, 140 °C, and 160 °C. The characteristic peak crystal surface index of the lithium-rich material is indicated on the XRD pattern of the obtained lithium-rich material. The peaks in the map are strong and sharp, and no impurity peaks indicate better crystallinity and pure phase content. The obvious splitting of the (006)/(102) and (108)/(110) peaks in the XRD spectrum indicates that the material has a good layered structure [3, 20, 21]. In Fig. 2, the two peaks at a drying temperature of 140 °C are

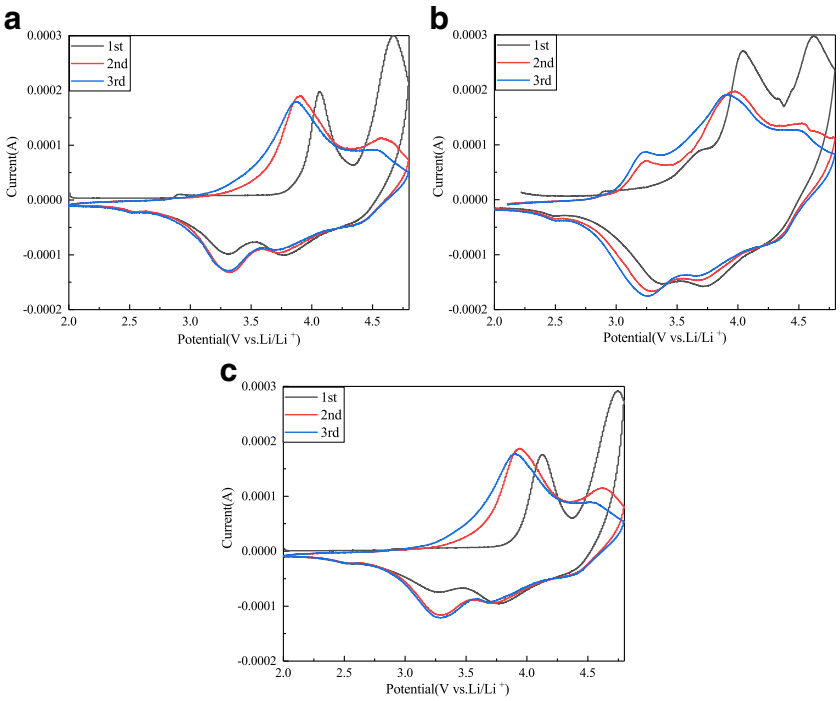

Fig. 6 Cyclic voltammetry (CV) curves at different drying temperatures. (a)120 °C. (b)140 °C. (c)160 °C

clearly split, indicating that the material has an excellent layered structure.

Table 1 shows the variation in lattice constants, *a* and *c*, and *c*/*a* ratio of $Li_{1.2}Mn_{0.54}Ni_{0.13}Co_{0.13}O_2$. The layered structure and cation disorder can be measured by the intensity ratio of (003) to (104) peak ($I_{(003)}/I_{(104)}$) and lattice parameter ratio of *c* to *a* (*c*/*a*). The value of $I_{(003)}/I_{(104)} < 1.2$ indicates that the cation mixing is not ideal [22–24]. It can be seen from Table 1 that the ratio of the three materials $I_{(003)}/I_{(104)}$ prepared is all greater than 1.2, and the ratio of the drying temperature to 140 °C is up to 1.64. Therefore, the degree of cation mixing is the lowest at 140 °C, and its performance is optimal.

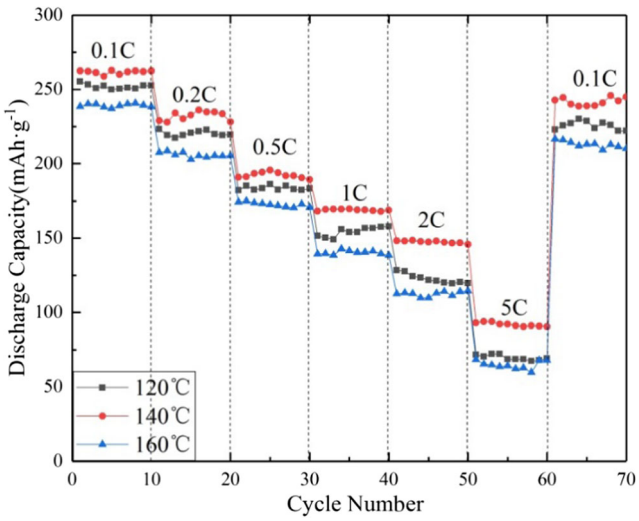

Fig. 7 The rate capability of samples synthesized with different drying temperature

Morphological observation

The particle size and morphology surface of the electrode material are related to their electrochemical performances. Figure 3 shows the SEM and TEM images of the $Li_{1.2}Mn_{0.54}Ni_{0.13}Co_{0.13}O_2$ samples. It can be clearly seen from the SEM image that the powders have similar morphology, smooth surface, uniform size, and uniform distribution. In addition, the smaller particle size means that the larger specific surface area of the material and the contact area of the electrolyte are larger, so that more and more metal ions can participate in the electrochemical reaction, effectively reducing the polarization of the electrode, and facilitating the rapid transmission of lithium ions [7, 25, 26]. It can be seen from the figure that the sample has a particle size between 100 and 300 nm at a drying temperature of 140 °C, which is more conducive to ion transport and thus has the best performance.

Figure 4 is an EDS spectrum of the lithium-rich positive electrode material particles based on the inset of Fig. 3 In the figure, nickel, cobalt, and manganese are evenly distributed and coincide with each other. As shown in Fig. 4, the chemical is directly related to the strength of the element [24, 27]. The EDS element mapping image clearly display that the Ni, Co, and Mn elements are equably distributed in the $Li_{1.2}Mn_{0.54}Ni_{0.13}Co_{0.13}O_2$ sample.

Electrochemical performances

Compared with traditional cathode materials, the biggest difference between lithium-rich manganese-based cathode

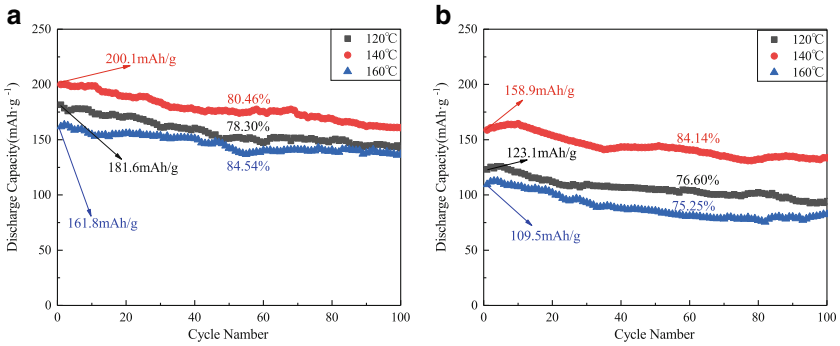

Fig. 8 Cycle performance of the different drying temperature materials. (**a**) 0.5 C. (**b**) 2 C

materials is the change in the first charge–discharge curve. As shown in Fig. 5, the first charge and discharge curves at different drying temperatures are at 0.1 C. The charging curve in the figure is mainly divided into two regions; the S-shaped curve below 4.5 V and the L-shaped platform above 4.5 V. The former is formed by the redox of Ni^{2+}/Ni^{4+} and Co^{3+}/Co^{4+} from $LiMn_{1/3}Ni_{1/3}Co_{1/3}O_2$. The latter is considered to be Li^+ from the layered Li_2MnO_3 structure, and with the release of O^{2-}, the final release is in the form of Li_2O [2, 28, 29]. It can be seen from Fig. 5 that the charge–discharge specific capacity is the largest when the drying temperature is 140 °C. The high specific capacity of 262.5 mAh/g corresponds to the previous crystal structure and morphology.

Figure 6 is a graph showing a capacity differential curve corresponding to the above figure. An important feature is the difference between the first cycle and the subsequent cycle. The first oxidation process has an oxidation peak near 4.6 V, which is related to the irreversible capacity loss at the first charge [19]. The two oxidation peaks appearing on the first cycle are 3.9 V and 4.6 V, which may be due to the oxidation of Ni^{2+} and Co^{3+} in the structure and the removal of Li^+ ions, accompanied by the release of oxygen. In the later stage, two distinct reduction peaks of about 3.7 V and 3.3 V can be clearly seen, which can be attributed to the reduction of Ni^{3+} and Mn^{4+} [30, 31], respectively. The oxidation peak of 4.6 V in the first cycle is obvious and sharp, mainly because Li^+ is continuously released with the release of oxygen, and finally precipitates from the Li_2MnO_3 component of the material in the form of Li_2O. The oxidation peak disappears in the next cycle, indicating that the reaction is irreversible [32]. The ratio of the oxidation peak current $I_{(4.6\ V)}/I_{(3.9\ V)}$ is related to the stability of the structure, and the lower $I_{(4.6\ V)}/I_{(3.9\ V)}$ value indicates that the structure is more stable. Obviously, the sample structure with a drying temperature is equal to 140 °C is the most stable [33].

Figure 7 shows the rate performance of $Li_{1.2}Mn_{0.54}Ni_{0.13}Co_{0.13}O_2$ at a drying temperature of 120 °C, 140 °C, and 160 °C. The electrochemical test voltage was set between 2.0 and 4.8 V, and the charge and discharge tests were carried out at different current densities of 0.1 C, 0.2 C, 0.5 C, 1 C, 2 C, and 5 C, and returned to 0.1 C (1 C = 200 mAh/g). The discharge capacity of these materials varies greatly at different rates, especially at large rates of 2 C and 5 C. The discharge specific capacity of the material at 140 °C is obviously the best at each drying temperature. The sample has a good rate performance associated with the particle size of the material. When the particle size is small, the path of lithium-ion migration inside the material is short and the diffusion area is large, which facilitates the rapid insertion and removal of lithium ions [7, 20, 34].

The cycle performance of as-prepared materials is presented in Fig. 8. The figure shows the discharge specific capacity of the battery under the cycle of 0.5 C and 2 C, respectively. With the extension of the 3.5 V high voltage, the discharge specific capacity of the sample gradually increases in the first 3 cycles, indicating that the Li_2MnO_3 phase takes several cycles to fully activate [11]. Among them, the best initial discharge specific capacity at 0.5 C and 2 C reaches 200.1 mAh/g

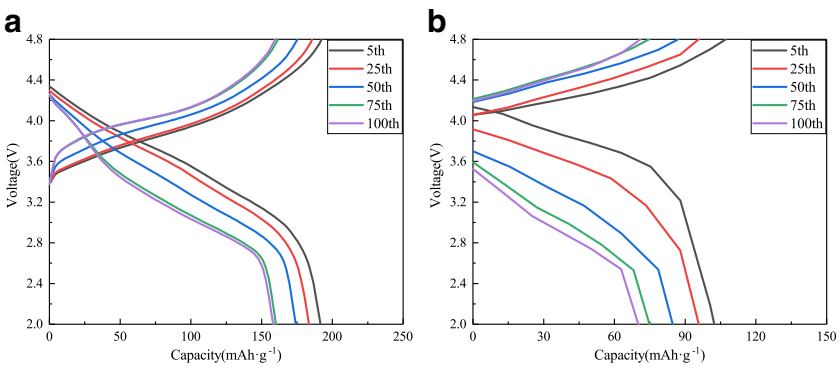

Fig. 9 Charge–discharge curves of the samples at drying temperature of 140 °C. (**a**) 1 C. (**b**) 5C

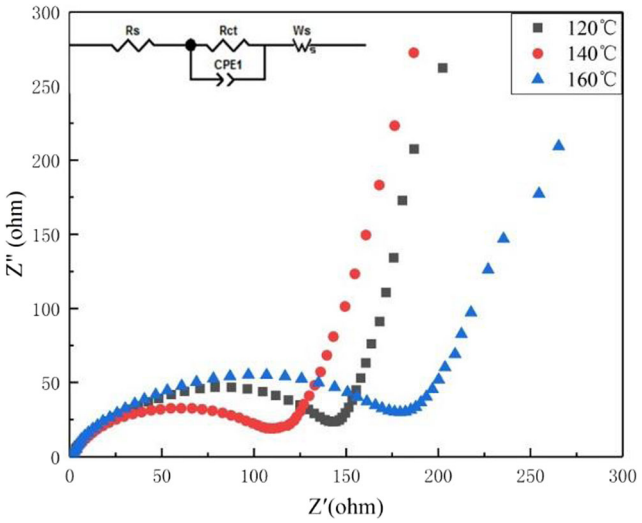

Fig. 10 AC impedance of samples synthesized with different drying temperature

and 158.9 mAh/g, respectively. The discharge specific capacity of each sample was attenuated as the number of cycles increased, but the performance was most excellent when the drying temperature was 140 °C with respect to the rest of the conditions. Figure 9 shows charge and discharge capacity plots for the 5th, 25th, 50th, 75th, and 100th cycles at 1 C and 5 C rates.

In order to fully study the effect of drying temperature on the resistance of Li^+ de$^-$/intercalation, all samples were tested for AC impedance in the uncharged cycle, as shown in Fig. 10. As can be seen from Fig. 10, the impedance map of all material samples consists of two parts: the semicircle of the high frequency region and the diagonal of the low frequency region. The migration impedance (R_s) of lithium ions inside the electrolyte is represented by the semicircular intercept of the high-frequency region and the real axis of the impedance; the semicircular diameter of the high-frequency region corresponds to the charge transfer impedance (R_{ct}); the oblique line of the low-frequency region that is used by Warburg impedance indicates that the impedance is related to the diffusion process of lithium ions inside the material, expressed in W_s [11, 35]. It can be seen from Table 2 that the sample has the lowest charge transfer impedance after drying at 140 °C, indicating that lithium ions can be rapidly de-intercalated at the material interface, which is consistent with the rate performance test results [36–38].

Table 2 The values of R_s and R_{ct} for as-prepared electrodes

Samples	120 °C	140 °C	160 °C
R_s (±Ω)	1.86	2.22	1.70
R_{ct} (±Ω)	140.92	106.70	177.68

Conclusions

In conclusion, the lithium-rich manganese-based $Li_{1.2}Mn_{0.54}Ni_{0.13}Co_{0.13}O_2$ cathode material was prepared by sol-gel method. A comparative analysis of three materials was carried out by controlling the drying temperature. XRD results show that the drying temperature has a significant effect on the layer structure and cation mixing degree of the material. The material structure with a drying temperature equal to 140 °C was found to be the most stable by CV test. Electrochemical test results show that the electrochemical performance of $Li_{1.2}Mn_{0.54}Ni_{0.13}Co_{0.13}O_2$ material is better when the drying temperature is 140 °C. It delivered the largest initial discharge capacity of 262.5 mAh/g and coulombic efficiency of 77.66% at 0.1 C. Furthermore, it showed a high discharge capacity of 200.1 mAh/g and 158.9 mAh/g at 0.5 C and 2 C and capacity retention of 80.46% and 84.14% after 100 cycles, respectively. We hope that the work done in this paper will play an important role in the further development of lithium-rich manganese-based materials.

Funding information This work was financially supported by the National Natural Science Foundation of China (Grant No.11264023) and the Natural Science Foundation of Gansu Province, China (Grant No. 1210ZTC035).

References

1. Shi J-L, Xiao D-D, Zhang X-D, Yin Y-X, Guo Y-G, Gu L, Wan L-J (2017) Improving the structural stability of Li-rich cathode materials via reservation of cations in the Li-slab for Li-ion batteries. Nano Res 10:4201–4209
2. Yi T-F, Tao W, Chen B, Zhu Y-R, Yang S-Y, Xie Y (2016) High-performance $xLi_2MnO_3{\cdot}(1\text{-}x)LiMn_{1/3}Co_{1/3}Ni_{1/3}O_2 (0.1 \le x \le 0.5)$ as cathode material for Lithium-ion battery. Electrochim Acta 188: 686–695
3. Kong J-Z, Zhai H-F, Qian X, Wang M, Wang Q-Z, Li A-D, Li H, Zhou F (2017) Improved electrochemical performance of $Li_{1.2}Mn_{0.54}Ni_{0.13}Co_{0.13}O_2$ cathode material coated with ultrathin ZnO. J Alloys Compd 694:848–856
4. Zhang Y, Li Y, Niu X, Wang D, Zhou D, Wang X, Gu C, Tu J (2015) A peanut-like hierarchical micro/nano-$Li_{1.2}Mn_{0.54}Ni_{0.18}Co_{0.08}O_2$ cathode material for lithium-ion batteries with enhanced electrochemical performance. J Mater Chem A 3:14291–14297
5. Su W, Feng W, Cao Y (2018) Porous honeycomb-like carbon prepared by a facile sugar- blowing method for high-performance lithium-sulfur batteries. Int J Electrochem Sci 13:6005–6014
6. Takahashi Y, Tode S, Kinoshita A, Fujimoto H, Nakane I, Fujitani S (2008) Development of lithium-ion batteries with a $LiCoO_2$ cathode toward high capacity by elevating charging potential. J Electrochem Soc 155:A537
7. Tang T, Zhang H-L (2016) Synthesis and electrochemical performance of lithium-rich cathode material Li $[Li_{0.2}Ni_{0.15}Mn_{0.55}Co_{0.1\text{-}x}Al_x]O_2$. Electrochim Acta 191:263–269
8. Liu HS, Zhang ZR, Gong ZL, Yang Y (2004) Origin of deterioration for $LiNiO_2$ cathode material during storage in air. Electrochem Solid-State Lett 7:A190
9. Yuan L-X, Wang Z-H, Zhang W-X, Hu X-L, Chen J-T, Huang Y-H, Goodenough JB (2011) Development and challenges of $LiFePO_4$

cathode material for lithium-ion batteries. Energy Environ Sci 4: 269–284
10. Lee H-W, Muralidharan P, Ruffo R, Mari CM, Cui Y, Kim DK (2010) Ultrathin spinel $LiMn_2O_4$ nanowires as high power cathode materials for Li-ion batteries. Nano Lett 10:3852–3856
11. Liu H, Chen C, Du C, He X, Yin G, Song B, Zuo P, Cheng X, Ma Y, Gao Y (2015) Lithium-rich $Li_{1.2}Ni_{0.13}Co_{0.13}Mn_{0.54}O_2$ oxide coated by Li_3PO_4 and carbon nanocomposite layers as high performance cathode materials for lithium ion batteries. J Mater Chem A 3:2634–2641
12. Yin H, Ji S, Gu M, Zhang L, Liu J (2015) Scalable synthesis of $Li_{1.2}Mn_{0.54}Ni_{0.13}Co_{0.13}O_2$ /$LiNi_{0.5}Mn_{1.5}O_4$ sphere composites as stable and high capacity cathodes for Li-ion batteries. RSC Adv 5:84673–84679
13. Wu F, Wang Z, Su Y, Yan N, Bao L, Chen S (2014) Li $[Li_{0.2}Mn_{0.54}Ni_{0.13}Co_{0.13}]O_2$–$MoO_3$ composite cathodes with low irreversible capacity loss for lithium ion batteries. J Power Sources 247:20–25
14. He W, Yuan D, Qian J, Ai X, Yang H, Cao Y (2013) Enhanced high-rate capability and cycling stability of Na-stabilized layered $Li_{1.2}[Co_{0.13}Ni_{0.13}Mn_{0.54}]O_2$ cathode material. J Mater Chem A 1: 11397
15. He W, Qian J, Cao Y, Ai X, Yang H (2012) Improved electrochemical performances of nanocrystalline Li $[Li_{0.2}Mn_{0.54}Ni_{0.13}Co_{0.13}]O_2$ cathode material for Li-ion batteries. RSC Adv 2:3423
16. Bai Y, Li Y, Wu C, Lu J, Li H, Liu Z, Zhong Y, Chen S, Zhang C, Amine K, Wu F (2015) Lithium-rich nanoscale $Li_{1.2}Mn_{0.54}Ni_{0.13}Co_{0.13}O_2$ cathode material prepared by co-precipitation combined freeze drying (CP-FD) for lithium-ion batteries. Energy Technol 3:843–850
17. Zhang L, Jin K, Wang L, Zhang Y, Li X, Song Y (2015) High capacity $Li_{1.2}Mn_{0.54}Ni_{0.13}Co_{0.13}O_2$ cathode materials synthesized using mesocrystal precursors for lithium-ion batteries. J Alloys Compd 638:298–304
18. Kim MC, Nam K-W, Hu E, Yang X-Q, Kim H, Kang K, Aravindan V, Kim W-S, Lee Y-S (2014) Sol-gel synthesis of aliovalent vanadium-doped $LiNi_{0.5}Mn_{1.5}O_4$ cathodes with excellent performance at high temperatures. ChemSusChem 7:829–834
19. Shin S-S, Sun Y-K, Amine K (2002) Synthesis and electrochemical properties of Li $[Li_{(1-2x)/3}Ni_xMn_{(2-x)/3}]O_2$ as cathode materials for lithium secondary batteries. J Power Sources 112:634–638
20. Xu H, Deng S, Chen G (2014) Improved electrochemical performance of $Li_{1.2}Mn_{0.54}Ni_{0.13}Co_{0.13}O_2$ by mg doping for lithium ion battery cathode material. J Mater Chem A 2:15015–15021
21. Xiang Y, Sun Z, Li J, Wu X, Liu Z, Xiong L, He Z, Long B, Yang C, Yin Z (2017) Improved electrochemical performance of $Li_{1.2}Ni_{0.2}Mn_{0.6}O_2$ cathode material for lithium ion batteries synthesized by the polyvinyl alcohol assisted sol-gel method. Ceram Int 43:2320–2324
22. Shaju K, Rao GS, Chowdari BV (2002) Performance of layered Li $(Ni_{1/3}Co_{1/3}Mn_{1/3})O_2$ as cathode for Li-ion batteries. Electrochim Acta 48:145–151
23. Jiao LF, Zhang M, Yuan HT, Zhao M, Guo J, Wang W, Zhou XD, Wang YM (2007) Effect of Cr doping on the structural, electrochemical properties of Li $[Li_{0.2}Ni_{0.2-x/2}Mn_{0.6-x/2}Cr_x]O_2$ (x=0, 0.02, 0.04, 0.06, 0.08) as cathode materials for lithium secondary batteries. J Power Sources 167:178–184
24. Kong J-Z, Wang C-L, Qian X, Tai G-A, Li A-D, Wu D, Li H, Zhou F, Yu C, Sun Y, Jia D, Tang W-P (2015) Enhanced electrochemical performance of $Li_{1.2}Mn_{0.54}Ni_{0.13}Co_{0.13}O_2$ by surface modification with graphene-like lithium-active MoS_2. Electrochim Acta 174: 542–550
25. Li L, Xu M, Chen Z, Zhou X, Zhang Q, Zhu H, Wu C, Zhang K (2015) High-performance lithium-rich layered oxide materials: effects of chelating agents on microstructure and electrochemical properties. Electrochim Acta 174:446–455
26. Zhang X, Yu C, Huang X, Zheng J, Guan X, Luo D, Li L (2012) Novel composites Li $[Li_xNi_{0.34-x}Mn_{0.47}Co_{0.19}]O_2$ ($0.18 \le x \le 0.21$): synthesis and application as high-voltage cathode with improved electrochemical performance for lithium ion batteries. Electrochim Acta 81:233–238
27. Xue Q, Li J, Xu G, Zhou H, Wang X, Kang F (2014) In situ polyaniline modified cathode material Li $[Li_{0.2}Mn_{0.54}Ni_{0.13}Co_{0.13}]O_2$ with high rate capacity for lithium ion batteries. J Mater Chem A 2:18613–18623
28. Zheng J, Gu M, Genc A, Xiao J, Xu P, Chen X, Zhu Z, Zhao W, Pullan L, Wang C, Zhang J-G (2014) Mitigating voltage fade in cathode materials by improving the atomic level uniformity of elemental distribution. Nano Lett 14:2628–2635
29. Wang Z, Luo S, Ren J, Wang D, Qi X (2016) Enhanced electrochemical performance of Li-rich cathode Li $[Li_{0.2}Mn_{0.54}Ni_{0.13}Co_{0.13}]O_2$ by surface modification with lithium ion conductor Li 3 PO 4. Appl Surf Sci 370:437–444
30. Kim J (2003) Synthesis and electrochemical behavior of Li $[Li_{0.1}Ni_{0.35-x/2}Co_xMn_{0.55-x/2}]O_2$ cathode materials. Solid State Ionics 164:43–49
31. Liu Y, Ning D, Zheng L, Zhang Q, Gu L, Gao R, Zhang J, Franz A, Schumacher G, Liu X (2018) Improving the electrochemical performances of Li-rich $Li_{1.20}Ni_{0.13}Co_{0.13}Mn_{0.54}O_2$ through a cooperative doping of Na^+ and PO_4^{3-} with Na_3PO_4. J Power Sources 375: 1–10
32. Johnson CS, Li N, Lefief C, Vaughey JT, Thackeray MM (2008) Synthesis, characterization and electrochemistry of lithium battery electrodes: $xLi_2MnO_3 \cdot (1-x)LiMn_{0.333}Ni_{0.333}Co_{0.33}O_2$ ($0 \le x \le 0.7$). Chem Mater 20:6095–6106
33. Wang YX, Shang KH, He W, Ai XP, Cao YL, Yang HX (2015) Magnesium-doped $Li_{1.2}[Co_{0.13}Ni_{0.13}Mn_{0.54}]O_2$ for lithium-ion battery cathode with enhanced cycling stability and rate capability. ACS Appl Mater Interfaces 7:13014–13021
34. Cao Y, Feng W, Su W (2018) Biosynthesis and characterization of $LiFePO_4$/C composite using Baker's yeast. Int J Electrochem Sci 13:8022–8029
35. Wang J, Yuan G, Zhang M, Qiu B, Xia Y, Liu Z (2012) The structure, morphology, and electrochemical properties of $Li_{1+x}Ni_{1/6}Co_{1/6}Mn_{4/6}O_{2.25+x/2}$ ($0.1 \le x \le 0.7$) cathode materials. Electrochim Acta 66:61–66
36. Yang H, Wu H, Ge M, Li L, Yuan Y, Yao Q, Chen J, Xia L, Zheng J, Chen Z, Duan J, Kisslinger K, Zhang Q, Lu J (2019) Simultaneously dual modification of Ni-rich layered oxide cathode for high-energy lithium-ion batteries. Adv Funct Mater 29:1808825
37. Li L, Chen Z, Zhang Q, Xu M, Zhou X, Zhu H, Zhang K (2015) A hydrolysis-hydrothermal route for the synthesis of ultrathin LiAlO2-inlaid LiNi0.5Co0.2Mn0.3O2 as a high-performance cathode material for lithium ion batteries. J Mater Chem A 3:894–904
38. Xiao B, Wang P-B, Zhang B, He Z-J, Yang Z, Tang L-B, An C-S, Zheng J (2018) Effect of MgO and TiO2 coating on electrochemical performance of Li-rich cathode materials for lithium-ion batteries. Energy Technology. https://doi.org/10.1002/ente.201800829